

Flat bands and enigma of metamagnetic quantum critical regime in $\text{Sr}_3\text{Ru}_2\text{O}_7$

V. R. Shaginyan,^{1,2,*} A. Z. Msezane,² K. G. Popov,³ J. W. Clark,⁴ M. V. Zverev,^{5,6} and V. A. Khodel^{5,4}

¹*Petersburg Nuclear Physics Institute, Gatchina, 188300, Russia*

²*Clark Atlanta University, Atlanta, GA 30314, USA*

³*Komi Science Center, Ural Division, RAS, Syktyukar, 167982, Russia*

⁴*McDonnell Center for the Space Sciences & Department of Physics, Washington University, St. Louis, MO 63130, USA*

⁵*Russian Research Centre Kurchatov Institute, Moscow, 123182, Russia*

⁶*Moscow Institute of Physics and Technology, Moscow, 123098, Russia*

Understanding the nature of field-tuned metamagnetic quantum criticality in the ruthenate $\text{Sr}_3\text{Ru}_2\text{O}_7$ has presented a significant challenge within condensed matter physics. It is known from experiments that the entropy within the ordered phase forms a peak, and is unexpectedly higher than that outside, while the magnetoresistivity experiences steep jumps near the ordered phase. We find a challenging connection between $\text{Sr}_3\text{Ru}_2\text{O}_7$ and heavy-fermion metals expressing universal physics that transcends microscopic details. Our construction of the $T - B$ phase diagram of $\text{Sr}_3\text{Ru}_2\text{O}_7$ permits us to explain main features of the experimental one, and unambiguously implies an interpretation of its extraordinary low-temperature thermodynamic in terms of fermion condensation quantum phase transition leading to the formation of a flat band at the restricted range of magnetic fields B . We show that it is the flat band that generates both the entropy peak and the resistivity jumps at the QCPs.

PACS numbers: 71.27.+a, 74.70.Pq, 71.10.Hf

Key Words: Quantum phase transitions; Heavy fermions; Flat bands, Residual resistivity, Metamagnetic transitions; Remnant entropy

Corresponding author: V. R. Shaginyan at: Petersburg Nuclear Physics Institute, Gatchina, 188300, Russia; Phones: (office) 7-813-714-6096, (fax) 7-813-713-1963; E-mail address: vrshag@thd.pnpi.spb.ru

I. INTRODUCTION

Discoveries of surprising and exotic phenomena in strongly correlated metals provide unique opportunities for expanding our understanding of quantum critical physics. A case in point is the quantum critical metal $\text{Sr}_3\text{Ru}_2\text{O}_7$, a member of the Ruddlesden-Popper series of layered perovskite ruthenates consisting of RuO_2 ab planes forming bilayers which are piled along the crystalline c axis, perpendicular to the ab axis, and weakly coupled to one another. In spite of numerous experimental and theoretical investigations [1–12], explanation of the puzzling low-temperature behavior of this material in external magnetic fields B remains an open problem in condensed matter theory, for recent reviews see e.g. [13, 14]. The observations indicate that the physics underlying this behavior of $\text{Sr}_3\text{Ru}_2\text{O}_7$, which resembles that of some heavy-fermion (HF) metals, is not subsumed in the spin-Kondo picture [7–9]. In crystals of high quality with residual resistivity $\rho_{\text{res}} \sim 0.4 \mu\Omega \text{ cm}$ measured at zero B -field and mean free path approximately 3000 Å, one observes a metamagnetic transition featuring a sud-

den and sharp rise in the magnetization \mathbf{M} with a modest increase in the applied field [13, 14], accompanied by a bifurcation of the metamagnetic phase boundary. At low temperatures the bifurcation splits into two first-order metamagnetic transitions at critical magnetic field values $B_{c1} \simeq 7.8 \text{ T}$ and $B_{c2} \simeq 8.1 \text{ T}$ [2, 3, 13, 14]. Conventionally, a phase that emerges at fields $B_{c1} < B < B_{c2}$ and temperatures $T \leq T_c \simeq 1.2 \text{ K}$ is identified as a nematic one [3, 4, 6]. This phase breaks the discrete square lattice rotational symmetry, as witnessed by a large magnetoresistive anisotropy in the ab plane as the magnetic field B is rotated away from the c axis toward the ab plane [3, 4]. The anisotropy vanishes as soon as the B -field is directed along the c axis (here we consider only this $B \parallel c$ case). The two first-order transitions persist, but convert into two second second-order phase transitions with rising temperature as illustrated in Fig. 1 A.

In our letter, we reveal a challenging connection between $\text{Sr}_3\text{Ru}_2\text{O}_7$ and heavy-fermion metals expressing universal physics that transcends microscopic details. Our construction of the $T - B$ phase diagram of $\text{Sr}_3\text{Ru}_2\text{O}_7$ permits us to explain main features of the experimental one. The obtained agreement with the experimental phase diagram is robust and does not depend on the nature of the ordered phase for our analysis is based on the thermodynamic consideration. We show that it is the flat band that generates both the entropy peak and the resistivity jumps at the QCPs. We reveal the nature of quantum critical points (QCPs) as associated with the fermion condensation quantum phase transition (FC-QPT) [15], and demonstrate that these steep jumps are represented by jumps of irregular residual resistivity ρ_0^c due to the presence of flat band, generated by FCQPT

*Electronic address: vrshag@thd.pnpi.spb.ru

and leading to fermion condensation (FC), rather than by the ordered phase itself. The same QCPs make the entropy within the ordered phase form a peak and produce a scaling behavior of the thermodynamic functions strongly resembling that of HF metals.

II. MAGNETORESISTIVITY

The magnetoresistivity $\rho(B, T)$ as a function of field and temperature is frequently approximated by the formula

$$\rho(B, T) = \rho_{\text{res}} + \Delta\rho(B) + AT^n, \quad (1)$$

where $\Delta\rho$ is the correction to the resistivity produced by the field B and A is a T -independent coefficient. The index n takes the values 2 and 1, respectively, for Landau Fermi liquid (LFL) and non-Fermi liquid (NFL) states and values $1 \lesssim n \lesssim 2$ in the crossover region between them. Although both the resistivity anisotropy and the ordered phase are striking, the essential physics in $\text{Sr}_3\text{Ru}_2\text{O}_7$ seems to be that of a normal-phase electron fluid at fields $B < B_{c1}$ and $B > B_{c2}$, and at $T > T_c$ and $B_{c2} > B > B_{c1}$, i.e., outside of the ordered phase. Indeed, data on the low-temperature magnetoresistivity $\rho(B)$ with $B \parallel c$ collected for $\text{Sr}_3\text{Ru}_2\text{O}_7$ [3] show that large changes of $\rho(B)$ occur as the ordered phase is approached. The straight lines indicated by arrows in Fig. 1 **A**, crossing pentagon data points on the low-field side and diamonds on the high-field side, represent the functions $T_r^1(B)$ and $T_r^2(B)$, respectively. In reference to panel **B** of Fig. 1, which shows the resistivity versus field strength at a series of temperatures, the straight line of panel **A** crossing pentagons [respectively, diamonds] delineates the intersection with the solid [dashed] line appearing in panel **B**. It is seen from Fig. 1 panel **A**, that $T_r^1(B = B_{c1}) \simeq 0$ and $T_r^2(B = B_{c2}) \simeq 0$. Thus, these functions show that the low-temperature sides of $\rho(B)$ at $T \rightarrow 0$ approach the steep sidewalls of the first-order phase transitions depicted in Fig. 1 **A**. Accordingly $\rho(B)$ possesses two steep sidewalls as the critical fields B_{c1} and B_{c2} are approached at $T \rightarrow 0$, a behavior evident in both panels of Fig. 1.

The behavior at $B \simeq 7.9$ T and $T > T_c$ is equally striking in that ρ is precisely linear in T at least over the range $1.2 \leq T \lesssim 18$ K [9]. This fact allows us to estimate the irregular residual resistivity $\rho_0^c(B)$. To evaluate $\rho_0^c(B)$, we extrapolate the data on the resistivity ρ [3] to zero temperature as if the ordered phase were absent in the range $B_{c2} > B > B_{c1}$. In this way at $B = 7.9$ T one finds $\rho_0^c \sim 1.7 \mu\Omega \text{ cm}$, while the residual resistivity in the presence of the nematic phase is $\rho_0^{\text{nem}} \sim 2.0 \mu\Omega \text{ cm}$ in this range. On the other hand, at $B \simeq 7.6$ T the residual resistivity is $\rho_0^c(B) \simeq 1.1 \mu\Omega \text{ cm}$. Thus, even in the absence of the ordered phase, the field B triggers an upward jump of the resistivity upon approaching B_{c1} from below. The resistivity is approximately constant in the range $B_{c1} < B < B_{c2}$ and undergoes a second

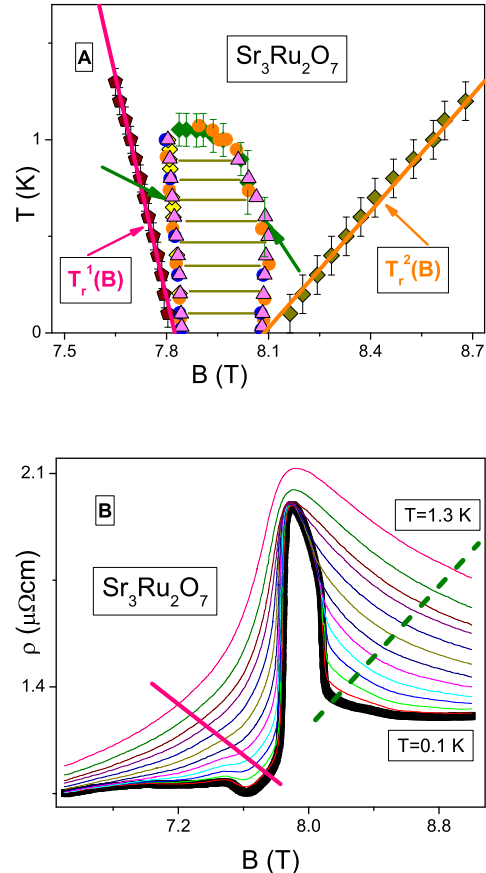


FIG. 1: (Color online). Panel **A**. Experimental phase diagram of $\text{Sr}_3\text{Ru}_2\text{O}_7$ in the $T - B$ plane with magnetic field B as the control parameter. Geometric symbols representing data points derived from measurements of susceptibility, magnetostriction, thermal expansion and transport measurements, surround an area cross-hatched with horizontal lines representing transitions between equilibrium thermodynamic phases associated with a nematic ordered phase [3, 4]. This phase is entered by first-order phase transitions at low temperatures (indicated by arrows) and by second-order phase transitions at high temperatures. The solid lines labeled with $T_r^1(B)$ and $T_r^2(B)$ on the low- and the high-field sides of the plot, respectively, sketch the temperature-field dependence $T_r^1(B)$ and $T_r^2(B)$ of the crossings of the resistivity $\rho(B, T)$ drawn in panel **B** with the two straight lines shown in the same panel. Panel **B**. The measured resistivity [3] $\rho(B)$ of $\text{Sr}_3\text{Ru}_2\text{O}_7$ at a series of temperatures between 0.1 and 1.3 K, in steps of 100 mK. The two lines cross the curves $\rho(B)$ at points symbolized by pentagons and diamonds in panel **A** and define the crossings $T_r^1(B)$ and $T_r^2(B)$, respectively.

jump downward as B approaches B_{c2} . Such behavior, seen at the lowest accessible temperatures of 15 mK [16] and 70 mK [17], at which the term AT^n in Eq. (1) can be safely omitted, is consistent with both the jumps at QCPs and the constancy in the range $B_{c1} < B < B_{c2}$ of

the irregular *residual* resistivity ρ_0^c . We conclude that it is ρ_0^c that are responsible for the observed behavior of ρ .

Let us assess possible causes for the jumps. When considering spin-orbit coupling in disordered electron systems where electron motion is diffusive, the residual resistivity may have both positive (weak localization) and negative (weak anti-localization) signs [18]. However, since $\text{Sr}_3\text{Ru}_2\text{O}_7$ exhibits successive upward and downward jumps separated by the narrow range of magnetic fields $B_{c2} - B_{c1}$, it is unclear how weak localization at B_{c1} is changed to weak anti-localization at B_{c2} . Moreover, $\text{Sr}_3\text{Ru}_2\text{O}_7$ is one of the purest metals and the applicable regime of electron motion is ballistic rather than diffusive. Therefore, both weak and anti-weak localization scenarios are irrelevant. Accordingly, one expects the B -dependent correction $\Delta\rho$ to the residual resistivity to be positive and small. As we have seen, this is far from the case.

Proposals for the origin of the jumps at finite temperatures may invoke band electrons close to a van Hove singularity (vHs), giving rise to the ordered phase [2, 4, 7, 11, 13, 14]. However, such scenarios must be rejected, since the electrons involved must have very large effective mass M^* and hence contribute only weakly to transport properties at finite temperatures and not at all at $T = 0$, see e.g. Ref. 7. Another possible source of the observed jumps might be resistivity associated with nematic domains that are thought to exist at $T \leq T_c$ for the fields tuning the system to a vHs [4, 7, 19, 20]. The jumps would be due to the extra scattering produced by such domains. This scenario is also problematic, since the domains would have to be present at least in the normal phase and at temperatures as high as $T \sim 18$ K, while the critical temperature for formation of both the nematic phase and the domains is estimated as $T_c \simeq 1.2$ K [4, 19, 20]. Failing such conventional explanations, we are faced with a challenging task that may well have broad implications for our understanding of unorthodox (notably, NFL) phenomena condensed-matter systems: how does one unveil the QCPs that create the quantum critical regime of $\text{Sr}_3\text{Ru}_2\text{O}_7$, giving rise to the emergence of jumps in the resistivity ρ_0^c and generating the entropy peak?

III. FERMION CONDENSATION

In order to develop viable explanations of the resistivity jumps and entropy excess, it is necessary to recall the origin, nature, and consequences of *flattening* of single-particle excitation spectra $\varepsilon(\mathbf{p})$ (“flat bands”) in strongly correlated Fermi systems – also called swelling of the Fermi surface or FC [21–25] (for recent reviews, see [15, 26, 27]). At $T = 0$, the ground state of a system with a flat band is degenerate, and the occupation numbers $n_0(\mathbf{p})$ of single-particle states belonging to the flat band are continuous functions of momentum \mathbf{p} , in contrast to discrete standard LFL values 0 and 1. Such behavior

of the occupation numbers leads to a T -independent entropy term

$$S_0 = - \sum_{\mathbf{p}} [n_0(\mathbf{p}) \ln n_0(\mathbf{p}) + (1 - n_0(\mathbf{p})) \ln(1 - n_0(\mathbf{p}))] \quad (2)$$

that does not contribute to the specific heat $C(T) = TdS/dT$. Unlike the corresponding LFL entropy, which vanishes linearly as $T \rightarrow 0$, the term S_0 produces a T -independent thermal expansion coefficient [15, 28–30]. That T -independent behavior is observed in measurements on CeCoIn_5 [31–33] and $\text{YbRh}_2(\text{Si}_{0.95}\text{Ge}_{0.05})_2$ [34], while very recent measurements on $\text{Sr}_3\text{Ru}_2\text{O}_7$ indicate the same behavior [35, 36] and confirm the existence of flat bands [12]. In the theory of fermion condensation, the degeneracy of the NFL ground state is removed at any finite temperature, since the flat band acquires a small dispersion [23]

$$\varepsilon(\mathbf{p}) = T \ln \frac{1 - n_0(\mathbf{p})}{n_0(\mathbf{p})} \quad (3)$$

proportional to T . The occupation numbers n_0 of FC remain unchanged at relatively low temperatures and, accordingly, so does the entropy S_0 .

We now introduce these concepts to achieve a coherent picture of the quantum critical regime underlying the jump phenomena in $\text{Sr}_3\text{Ru}_2\text{O}_7$. In constructing a field-induced flat band, we employ the model [4, 6, 7, 11, 37, 38] based on a vHs that induces a peak in the single-particle density of states (DOS) and sharp rise of \mathbf{M} as the field sweeps across the metamagnetic transition. Upon increase of an applied magnetic field B , the vHs is moved through the Fermi energy. At fields in the range $B_{c1} < B < B_{c2}$ the DOS peak turns out to be at or near the Fermi energy. A key point in this scenario is that within the range $B_{c1} < B < B_{c2}$, a relatively weak repulsive interaction (e.g., Coulomb) is sufficient to induce FC and formation of a flat band with the corresponding DOS singularity locked in the Fermi energy [15, 26, 27, 39]. Now, it is seen from Eq. (3) that finite temperatures, while removing the degeneracy of the FC spectrum, do not change S_0 , threatening the violation of the Nernst theorem. To avoid such an entropic singularity, the FC state must be altered as $T \rightarrow 0$, so that the excess entropy S_0 is shed before zero temperature is reached. This can take place by means of some phase transition or crossover, whose explicit consideration is beyond the scope of this paper.

IV. PHASE DIAGRAM

The schematic $T - B$ phase diagram of $\text{Sr}_3\text{Ru}_2\text{O}_7$ inferred from the proposed scenario is presented in Fig. 2. Its main feature is the magnetic field-induced quantum critical domain created by QCPs situated at B_{c1} and B_{c2} and supporting a FC and associated flat band induced by a vHs (double-headed arrow between black dots). The

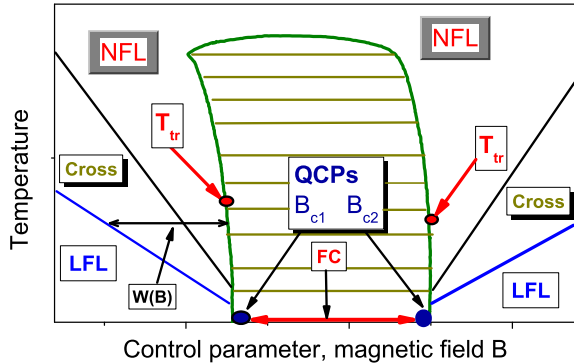


FIG. 2: (Color online). Schematic phase diagram of the metal $\text{Sr}_3\text{Ru}_2\text{O}_7$. The QCPs situated at the critical magnetic fields B_{c1} and B_{c2} are indicated by arrows. The fermion condensation (FC) or flat band is present between these QCPs as depicted by the double-headed arrow. The ordered phase bounded by the curve and demarcated by horizontal lines emerges to eliminate the entropy excess given by Eq. (2). Two arrows label the tricritical points T_{tr} at which the lines of second-order phase transitions change to the first order. The total width of the NFL state and the crossover leading to the LFL state, $W(B) \propto T$, is denoted by an arrow. The LFL state occurs at the lowest temperatures below and above the critical values B_{c1} and B_{c2} of the tuned B -field. Rising temperature ushers in a broad crossover (labeled Cross) from the LFL to the NFL state.

low-field [high-field] QCP on the left [right] augurs the emergence of the flat band as $B \rightarrow B_{c1}$ [$B \rightarrow B_{c2}$] from below [above]. In contrast to the typical phase diagram of a HF metal [15], the domain occupied by the ordered phase in Fig. 2 is seen to be approximately symmetric with respect to the magnetic field $B_c = (B_{c2} + B_{c1})/2$. The emergent FC and QCPs are considered to be hidden or concealed in a phase transition, which is driven by the need for the system to avoid the entropic singularity that would be produced at $T \rightarrow 0$ by the T -independent entropy term S_0 of Eq. (2). The area occupied by this phase transition is indicated by horizontal lines and restricted by boundary lines (“sidewalls” and “roof”). At the critical temperature T_c where the new (ordered) phase sets in, the entropy is a continuous function. Therefore the “roof” of the domain occupied by the new phase is a line of second-order phase transitions. As T is lowered, some temperature T_{tr} is reached at which the entropy of the ordered phase becomes larger than that of the adjacent disordered phase, due to the remnant entropy S_0 from the highly entropic flat-band state that is present above T_c . Therefore, under the influence of the magnetic field, the system undergoes a first-order phase transition upon crossing a sidewall boundary at $T = T_{tr}$, since entropy cannot be equalized there. It follows, then, that the line of second-order phase transitions is changed to a line of first-order transitions at tricritical points in-

dicated by arrows in Fig. 2. It is seen from Fig. 2 that the sidewall boundary lines are not strictly vertical, due to the stated behavior of the entropy at the boundary and as a consequence of the magnetic Clausius-Clapeyron relation [6, 7]. Indeed, in our case the Clausius-Clapeyron equation reads,

$$\mu_0 \frac{dB_{cn}}{dT_c} = -\frac{\Delta S}{\Delta M}. \quad (4)$$

Here, μ_0 is the permeability constant and B_{cn} stands for B_{c1} and B_{c2} . The beauty of Eq. (4) is that it defines the slope of the boundary lines shown in Fig. 2 from the first principles of thermodynamics. Since the entropy S within the bounded region is higher than that outside, the slopes of the phase boundaries point outwards as shown in Fig. 2. We conclude that the phase diagram 2 is in good agreement with the experimental one shown in Fig. 1, Panel A. We note that the obtained agreement is robust and does not depend on the nature of the ordered phase for our analysis is based on the thermodynamic consideration. For example, such a consideration allows one to establish the $T-B$ phase diagram of the HF metal CeCoIn_5 that resembles that of $\text{Sr}_3\text{Ru}_2\text{O}_7$ [30, 40].

On each flank of the region occupied by the ordered (nematic) phase, the system crosses over from the LFL state prevailing at the lowest temperatures to a NFL state under rising temperature. The total width $W(B)$ of the NFL state and crossover (“Cross”) region on either flank (denoted with a double arrow in Fig. 2), is proportional to T [30, 41]. The behavior of $W(B)$ inferred from this phase diagram is also reflected in Fig. 1 B, which depicts the dependence of the function $\rho(B)$ on field strength and temperature. Since the width $W(B)$ vanishes when the magnetic field tends to its critical values, $\rho(B)$ is represented by the two steep sidewalls seen in panel B of Fig. 1 as the critical field values B_{c1} and B_{c2} are respectively approached from below and above.

V. JUMPS

We turn next to calculations of the resistivity ρ in the range $B_{c1} < B < B_{c2}$, the dispersion of the flat band being governed by Eq. (3). The electronic liquid of $\text{Sr}_3\text{Ru}_2\text{O}_7$ is described by several bands occupied by normal quasiparticles that simultaneously intersect the Fermi surface, along with heavy quasiparticles whose dispersion never covers the entire Fermi surface [4, 6, 7, 11, 37, 38, 42]. Based on Eq. (3), the temperature dependence of the effective mass $M^*(T)$ of the FC quasiparticles is given by

$$M^*(T) \sim \frac{\eta p_F^2}{4T}, \quad (5)$$

where $\eta = \delta p/p_F$ is determined by the characteristic size δp of the momentum domain occupied by the FC and

p_F is the Fermi momentum [15, 26, 27]. From this relation it follows that the effective mass of FC quasiparticles diverges at low temperatures, while their group velocity, and hence their current, vanishes. Therefore the main contribution to the resistivity is provided by normal quasiparticles outside the FC having non-divergent effective mass M_L^* and finite group velocity at $T \rightarrow 0$. Nonetheless, it will be seen that FC quasiparticles still play a key role in determining the behavior of the irregular residual resistivity in the range $B_{c1} < B < B_{c2}$.

The resistivity has the conventional dependence [43]

$$\rho(T) \propto M_L^* \gamma \quad (6)$$

on the effective mass M_L^* and damping γ of the normal quasiparticles. Based on the relation (5), the behavior of γ is obtained in closed form in the present context as

$$\gamma \sim \eta(\gamma_0 + T), \quad (7)$$

where γ_0 is a constant [30, 41]. It is seen from Eq. (7) that the coefficient A on the right hand side of Eq. (1) is partly formed by FC. We call this contribution to A , coming from FC, A_{FC} .

We consider now additional contribution A_{TS} to the T -linear resistivity, formed by the zero sound generated by the presence of FC [44, 45]. The system with FC possesses its own set of zero-sound modes. The mode of interest for our analysis contributes to the T -linear dependence of the resistivity, as the conventional sound mode does in the case of normal metals [45]. The mode is that of transverse zero sound with its T -dependent sound velocity $c_t \simeq \sqrt{T/M_{vHs}}$ and the Debye temperature [44]

$$T_D \simeq c_t k_{max} \simeq \beta \sqrt{TT_F}. \quad (8)$$

Here, β is a factor, M_{vHs} is the effective mass of electron formed by vHs, T_F is the Fermi temperature, while M^* on the left hand side of Eq. (5) is the effective mass formed finally by some interaction, e.g. the Coulomb interaction, generating flat bands [39, 46]. The characteristic wave number k_{max} of the soft transverse zero-sound mode is estimated as $k_{max} \sim p_F$ since we assume that the main contribution forming the flat band comes from vHs. We note that the numerical factor β cannot be established and is considered as a fitting parameter, correspondingly, making T_D given by Eq. (8) uncertain. Estimating $T_F \sim 10$ K and taking $\beta \sim 0.3$, and observing that the quasi-classical regime takes place at $T > T_D \simeq \beta \sqrt{TT_F}$, we obtain that $T_D \sim 1$ K and expect that strongly correlated Fermi systems can exhibit a quasi-classical behavior with the low-temperature coefficient A , entering Eq. (1), $A = A_{FC} + A_{TS}$ [44, 45, 47].

Thus, in HF metals with their few bands crossing Fermi level and populated by LFL quasiparticles and by HF quasiparticles, the transverse zero sound make the resistivity possess the T -linear dependence at the quantum criticality as the normal sound (or phonons) do in the case of ordinary metals, while FC adds the quantum contribution A_{FC} to the coefficient A [45, 47]. The observed

contributions lead to the lifetime τ_q , formed by normal, FC quasiparticles, and the transverse zero sound,

$$\hbar/\tau_q \simeq a_1 + a_2 T, \quad (9)$$

where \hbar is Planck's constant, a_1 and a_2 are T -independent parameters. Relations (7) and (9) is in excellent agreement with recent experimental observations [48]. In playing its key role, the FC makes all quasiparticles possess the same unique width γ and lifetime τ_q . As we shall see, the T -independent width γ_0 forms the irregular residual resistivity ρ_0^c .

Using relations (1), (6) and (7) together with the standard treatment of vertex corrections [49], we are led to conclude that the resistivity of $\text{Sr}_3\text{Ru}_2\text{O}_7$ should behave as

$$\rho \sim \rho_{\text{res}} + \Delta\rho(B) + \rho_0^c + AT \quad (10)$$

in the thermodynamic regime in question. The term ‘‘residual resistivity’’ ordinarily refers to impurity scattering. In the present case, as seen from Eqs. (7) and (10), the irregular residual resistivity ρ_0^c is instead determined by the onset of a flat band, and has no relation to scattering of quasiparticles by impurities. Since the FC and the flat band manifest themselves on in the region $B_{c1} < B < B_{c2}$, it is natural also to conclude that the QCPs indicated in Fig. 2 are responsible for the jumps in the irregular residual resistivity ρ_0^c . According to the relations (7) and (10), the resistivity ρ is a linear function of T [30, 41]. This feature of the flat-band scenario is in accordance with the relevant measurements on $\text{Sr}_3\text{Ru}_2\text{O}_7$ [9]. Moreover, experimental observations and their theoretical explanation show that the same physics describes the T -linear dependence of the resistivity of conventional metals and both HF metals and $\text{Sr}_3\text{Ru}_2\text{O}_7$, with the quasi-classical behavior formed by the zero-sound mode at their quantum criticality [47, 50].

As it was discussed above, heavy quasiparticles shaped by the flat band do not contribute directly to the transport properties. Defining the lifetime τ_q instead, these specify the transport of the system. As a result, the magnetoresistivity jumps and its variation through the peak are defined by the variation of the irregular residual resistivity ρ_0^c . Indeed, increasing the temperature broadens and increases the resistivity in accordance with Eq. (10), but the minimal values of the jumps and of the peak exhibit the spectacular independence of temperature, as it is seen from Fig. 1 B. A salient experimental feature supporting this conclusion is the occurrence of two jumps in the resistivity: first an upward jump at B_{c1} , where the FC is built up, followed by a downward jump at B_{c2} , where the FC is destroyed. Thus, the scenario developed here reveals the genesis of the two steep sidewalls observed in the irregular residual resistivity ρ_0^c , in effects arising from the formation of a flat band at QCPs. One could attribute ρ_0^c to the influence of the magnetic field B , considering ρ_0^c as a magnetoresistivity. Such a definition would obscure the physical mechanism responsible

for forming ρ_0^c . Indeed, it is the flat band that forms the irregular residual resistivity, while the magnetic field represents an auxiliary parameter that tunes the system to the flat band.

VI. ENTROPY

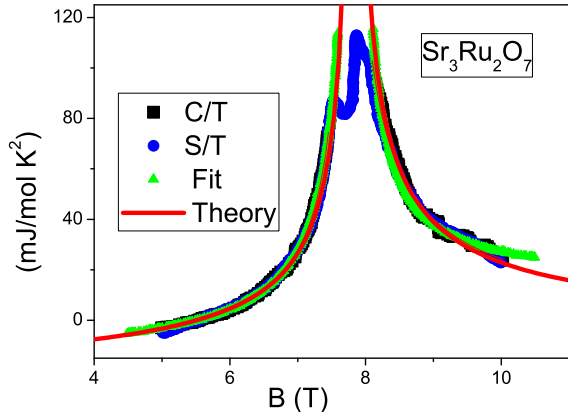


FIG. 3: (Color online). Magnetic-field dependence of both the specific heat C/T (depicted by the squares) and the entropy S/T (circles) as obtained in measurements on $\text{Sr}_3\text{Ru}_2\text{O}_7$ and their divergent behavior as fitted by the function $B_c|B - B_c|^\alpha$ with $\alpha = -1$ (triangles) [6]. The theoretical fit of the current work is shown as the solid curve given by Eq. (11).

In the LFL state depicted in Fig. 2, both the entropy S and the specific heat C of the electron liquid in $\text{Sr}_3\text{Ru}_2\text{O}_7$ behave in accordance with LFL theory $S/T = C/T \propto M^*$ [49], with the exception that the effective mass M^* depends on magnetic field B according to $M^*(B) \propto |B - B_c|^{-2/3}$ [15, 51]. Here, B_c is the field at which the QCP occurs; in the present case of two QCPs, B_c is taken equal to $B_c = (B_{c2} + B_{c1})/2 \simeq 7.9$ T, for simplicity. The entropy is then given by

$$S(B)/T = C/T \simeq A_s + D_s|B - B_c|^{-2/3}, \quad (11)$$

where A_s and D_s are fitting parameters for the low-field and high-field QCPs. The LFL behavior of C/T and S/T fitted by Eq. (11) are shown by the solid curve in Fig. 3, in comparison with experimental results [6] for these quantities represented by squares and circle symbols, respectively. The triangles display the fit with exponent $\alpha = -1$ [6] rather than $\alpha = -2/3$. The two fits (the solid curve and the triangles) are seen to show similar behavior as functions of magnetic field. In contrast to the exponent $\alpha = -1$ obtained by the fitting of the experimental data over small variation of the magnetic field [6], the validity of the exponent $\alpha = -2/3$ is then confirmed by the good agreement with the experimental data and internal consistency between the schematic

phase diagram in Fig. 2 and the data in Figs. 1, 3 and 4. Figure 3 shows that the entropy increases strongly on both the low-field and high-field sides of the ordered phase as the critical fields B_{c1} and B_{c2} are approached. Thus, the theory of FC allows us to explain, for the first time, the experimental data collected for $\text{Sr}_3\text{Ru}_2\text{O}_7$ [6, 36] on the evolution of the entropy and the heat capacity as the quantum critical point is approached. We note that the entropy jumps across the first-order phase transitions visible in Fig. 3 are in accord with the phase diagram sketched in Fig. 2.

VII. SCALING BEHAVIOR

With the aim of revealing signatures of the hidden QCPs, we conclude with an analysis of the thermodynamic properties of the C/T electronic specific heat measurements on $\text{Sr}_3\text{Ru}_2\text{O}_7$ [9]. As mentioned above, at $B = 7.9$ T the resistivity ρ is precisely linear in T over the range $T_c \leq T < 18$ K, with C/T varying as $\ln T$ over the same range [9]. These are typical fingerprints of a flat band generated by FC at QCPs [30, 41]. The experimentally derived temperature dependence of $C/T \propto M^*$ on magnetic field strength, shown in Fig. 4 A, allows us to uncover the universal scaling behavior of the effective mass M^* characteristic of HF metals. As shown in this figure, the maximum of $C/T \propto M^*$ sharpens and shifts to lower temperatures as the field B approaches 7.9 T, where the maximum disappears. In contrast to HF metals, C/T exhibits a symmetry with respect to the area implicated by the ordering (nematic) transition: the maximum appears upon approach to the QCPs and reappears on the high-field side of this transition region. This behavior of the maximum is in accord with the phase diagram of Fig. 2, since the width $W(B)$ increases linearly with T and the maximum located in the transition region shifts toward zero temperature, while the effective mass $M^*(B)$ given by Eq. (11) diverges as B approaches the critical field. To expose the scaling behavior, we normalize the measured C/T values to $(C/T)_N = (C/T)/(C/T)_M$ and the corresponding temperatures T to T_N , $T_N = T/T_M$, by dividing by their values T_M and $(C/T)_M$ at the maxima [15]. The elucidative values of T_M and $(C/T)_M$ at $B = 4$ T are depicted by the arrows in panel A of Fig. 4. The spin AC susceptibility data $\chi(T) \propto M^*$ are normalized in the same way. At FQCPT, all the normalized χ_N and $(C/T)_N$ curves are to merge into a single one, $\chi_N = (C/T)_N = M_N^*(T_N)$, where M_N^* is the normalized effective mass represented by a universal function, being a solution of the Landau equation [15]. This solution $M_N^*(T_N)$ can be well approximated by a simple universal interpolating function. The interpolation occurs between the LFL and NFL regimes and represents the universal scaling behavior of M_N^* [15]

$$M_N^*(T_N) \approx c_0 \frac{1 + c_1 T_N^2}{1 + c_2 T_N^{8/3}}. \quad (12)$$

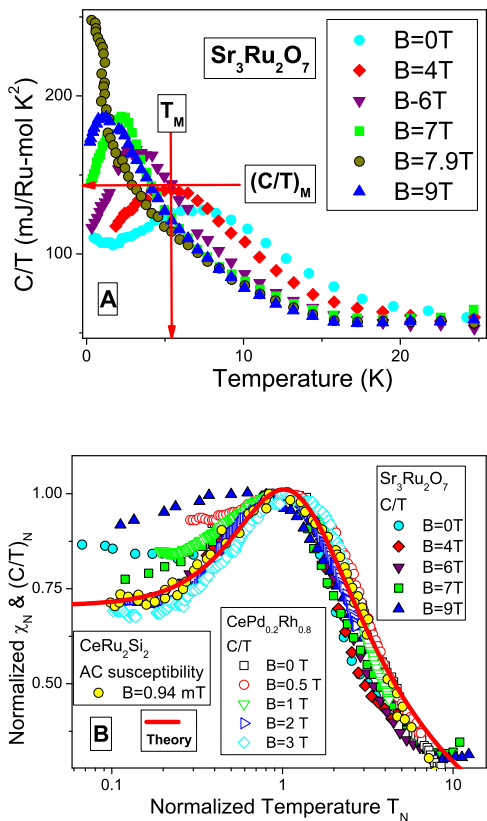


FIG. 4: (Color online). Panel **A**. Temperature dependence of the electronic specific heat for different magnetic field strengths (after Rost *et al.* [9]). The maximum at zero field increases and shifts to lower temperatures as the magnetic field approaches QCPs. At $B = 7.9$ T no maximum occurs. A maximum reappears on the high-field side of the transition, demonstrating a symmetrical behavior with respect the critical region located between the two QCPs and occupied by the ordered phase. The illustrative values of $(C/T)_M$ and T_M at $B = 4$ T are shown by the arrows. Panel **B**. Universal scaling behavior of the normalized specific heat $\chi_N = (C/T)_N \propto M^*$, extracted from measurements on CeRu_2Si_2 [52], $\text{CePd}_{1-x}\text{Rh}_x$ with $x = 0.80$ [53], and $\text{Sr}_3\text{Ru}_2\text{O}_7$ [9]. All the measurements displayed in panels **A** and **B** were performed under the application of magnetic fields as shown in the insets. The solid curve represents our calculation of the universal behavior.

Here, $c_0 = (1 + c_2)/(1 + c_1)$, c_1 , and c_2 are fitting parameters. Figure 4 **B** reports the behavior of the normalized

χ_N and $(C/T)_N$ thus extracted from measurements on CeRu_2Si_2 [52], $\text{CePd}_{0.8}\text{Rh}_{0.8}$ [53] and $\text{Sr}_3\text{Ru}_2\text{O}_7$ [9]. The solid curve shows the result of our calculation of the scaling behavior that can be well fit by Eq. (12). The HF metals and $\text{Sr}_3\text{Ru}_2\text{O}_7$ are seen to exhibit the same scaling behavior, which can be understood within the framework of fermion condensation or flat-band theory [15, 26, 27].

VIII. SUMMARY

In summary, we have unveiled a challenging connection between $\text{Sr}_3\text{Ru}_2\text{O}_7$ and heavy-fermion metals by establishing universal physics that straddles across the corresponding microscopic details. Our construction of the $T - B$ phase diagram of $\text{Sr}_3\text{Ru}_2\text{O}_7$ has permitted us to explain main features of the experimental one, and unambiguously implies an interpretation of its extraordinary low-temperature thermodynamic in terms of fermion condensation quantum phase transition leading to the formation of a flat band at the restricted range of magnetic fields $B_{c1} \leq B \leq B_{c2}$. We have demonstrated that the obtained agreement with the experimental phase diagram is robust and does not depend on the nature of the ordered phase, for our analysis is based on the thermodynamic consideration. We have shown that it is the flat band that generates both the entropy peak and the resistivity jumps, as the critical fields B_{c1} and B_{c2} are approached. We have also detected the scaling behavior of the thermodynamic functions of $\text{Sr}_3\text{Ru}_2\text{O}_7$ coinciding with that of heavy-fermion metals.

In the future, it would be interesting to analyze the physics of the ordered (nematic) phase. Our preliminary results show that the fermion condensation state breaks the discrete square lattice rotational symmetry and generates a large magnetoresistive anisotropy, as the magnetic field B is rotated away from the c axis toward the ab plane.

IX. ACKNOWLEDGEMENT

Stimulating discussions with P. Gegenwart are gratefully acknowledged. This work was supported by U.S. DOE, Division of Chemical Sciences, Office of Basic Energy Sciences, Office of Energy Research and AFOSR, and the McDonnell Center for the Space Sciences.

-
- [1] S. A. Grigera, et al., Science 294 (2001) 329.
 - [2] R. S. Perry, et al., Phys. Rev. Lett. 92 (2004) 166602.
 - [3] S. A. Grigera, et al., Science 306 (2004) 1154; J. A. N. Bruin, et al., Phys. Rev. B 87 (2013) 161106(R).
 - [4] R. A. Borzi, et al., Science 315 (2007) 214.
 - [5] J. Farrell, et al., Phys. Rev. B 78 (2008) 180409(R).
 - [6] A. W. Rost, et al., Science 325 (2009) 1360.
 - [7] S. Raghu, et al., Phys. Rev. B 79 (2009) 214402.
 - [8] J. Lee, et al., Nat. Phys. 5 (2009) 800.
 - [9] A. W. Rost, et al., Proc. Natl. Acad. Sci. 108 (2011) 16549.
 - [10] A. J. Millis, A. J. Schofield, G. G. Lonzarich, S. A. Grig-

- era, Phys. Rev. Lett. 88 (2002) 217204.
- [11] B. Binz, M. Sigrist, Europhys. Lett. 65 (2004) 816.
- [12] M. P. Allan, et al., New J. Phys. 15 (2013) 063029.
- [13] E. Fradkin, S. A. Kivelson, M. J. Lawler, J. P. Eisenstein, A. P. Mackenzie, Annu. Rev. Condens. Matter Phys. 1 (2010) 153.
- [14] A. P. Mackenzie, J. A. N. Bruin, R. A. Borzi, A. W. Rost, S. A. Grigera, Physica C 481 (2012) 207.
- [15] V. R. Shaginyan, M. Ya. Amusia, A. Z. Msezane, K. G. Popov, Phys. Rep. 492 (2010) 31.
- [16] F. Weickert, P. Gegenwart, R. S. Perry, Y. Maeno, Physica C 460-462 (2007) 520.
- [17] R. A. Borzi, et al., Phys. Rev. B 84 (2011) 205112.
- [18] S. Hikami, A. I. Larkin, Y. Nagaoka, Prog. Theor. Phys. 63 (1980) 707.
- [19] J.-F. Mercure, et al., Phys. Rev. Lett. 103 (2009) 176401.
- [20] C. Stingl, R. S. Perry, Y. Maeno, P. Gegenwart, Phys. Rev. Lett. 107 (2011) 026404.
- [21] V. A. Khodel, M. V. Zverev, V. M. Yakovenko, Phys. Rev. Lett. 95 (2005) 236402.
- [22] V. A. Khodel, V. R. Shaginyan, JETP Lett. 51 (1990) 553.
- [23] P. Nozières, J. Phys. I France 2 (1992) 443.
- [24] G. E. Volovik, Quantum Phase Transitions from Topology in Momentum Space, Lect. Notes in Physics 718 (2007) 31.
- [25] T. T. Heikkilä, N. B. Kopnin, G. E. Volovik, JETP Lett. 94 (2011) 233.
- [26] V. R. Shaginyan, Physics of Atomic Nuclei 74 (2011) 1107.
- [27] V. A. Khodel, J. W. Clark, M. V. Zverev, Physics of Atomic Nuclei 74 (2011) 1237.
- [28] M. V. Zverev, V. A. Khodel, V. R. Shaginyan, M. Baldo, JETP Lett. 65 (1997) 863.
- [29] M. Ya. Amusia, A. Z. Msezane, V. R. Shaginyan, Phys. Lett. A **320**, 459 (2004).
- [30] V. R. Shaginyan, A. Z. Msezane, K. G. Popov, J. W. Clark, M. V. Zverev, V. A. Khodel, Phys. Rev. B 86 (2012) 085147.
- [31] N. Oeschler et al., Phys. Rev. Lett. 91 (2003) 076402.
- [32] J. G. Donath, F. Steglich, E. D. Bauer, J. L. Sarrao, P. Gegenwart, Phys. Rev. Lett. 100 (2008) 136401.
- [33] S. Zaum, et al., Phys. Rev. Lett. 106 (2011) 087003.
- [34] R. KÜchler, et al., Phys. Rev. Lett. 91 (2003) 066405.
- [35] P. Gegenwart, F. Weickert, M. Garst, R. S. Perry, Y. Maeno, Phys. Rev. Lett. 96 (2006) 136402.
- [36] C. Stingl, R. S. Perry, Y. Maeno, P. Gegenwart, Phys. Status Solidi B 250 (2013) 450.
- [37] A. M. Berridge, S. A. Grigera, B. D. Simons, A. G. Green, Phys. Rev. B 81 (2010) 054429.
- [38] C. M. Puetter, J. G. Rau, H.-Y. Kee, Phys. Rev. B 81 (2010) 081105(R).
- [39] D. Yudin, et al., arXiv:1308.0812.
- [40] V. R. Shaginyan, A. Z. Msezane, V. A. Stephanovich, E. V. Kirichenko, Europhys. Lett. 76 (2006) 898.
- [41] V. R. Shaginyan, A. Z. Msezane, K. G. Popov, J. W. Clark, M. V. Zverev, V. A. Khodel, JETP. Lett. 96 (2012) 397.
- [42] A. Tamai, et al., Phys. Rev. Lett. 101 (2008) 026407.
- [43] D. Pines, P. Nozières, Theory of Quantum Liquids, Benjamin, New York, 1966.
- [44] V. A. Khodel, J. W. Clark, V. R. Shaginyan, M. V. Zverev, JETP Lett. 92 (2010) 532.
- [45] J. W. Clark, V. A. Khodel, M. V. Zverev, Phys. Lett. A 377 (2013) 647.
- [46] V. A. Khodel, J. W. Clark, H. Li, M. V. Zverev, Phys. Rev. Lett. 98 (2007) 216404.
- [47] V. R. Shaginyan, K. G. Popov, V. A. Khodel, arXiv:1304.2068.
- [48] P. Aynajian, et al., Nature 486 (2012) 201.
- [49] A. A. Abrikosov, L. P. Gor'kov, I. E. Dzyaloshinski, Methods of Quantum Field Theory in Statistical Physics, Prentice-Hall, London, 1963.
- [50] J. A. N. Bruin, H. Sakai, R. S. Perry, A. P. Mackenzie, Science 339 (2013) 804.
- [51] J. W. Clark, V. A. Khodel, M. V. Zverev, Phys. Rev. B 71 (2005) 012401.
- [52] D. Takahashi, et al., Phys. Rev. B 67 (2003) 180407(R).
- [53] A. P. Pikul, et al., J. Phys. Condens. Matter 18 (2006) L535.